IOS Press

Real-space computational methods for linear and nonlinear polarizabilities

Jun-Ichi Iwata[a,*], Kazuhiro Yabana[b] and George F. Bertsch[c]
[a]*Nanotechnology Research Institute, National Institute of Advanced Industrial Science and Technology (AIST), Tsukuba 305-8568, Japan*
[b]*Institute of Physics, University of Tsukuba, Tsukuba 305-8571, Japan*
[c]*Department of Physics and National Institute for Nuclear Theory, University of Washington, Seattle, Washington 98195, USA*

Abstract. We present a real-space method for computing the linear and nonlinear polarizabilities in the time-dependent density-functional theory. In our method, the three-dimensional Cartesian coordinate is discretized on a uniform grid and the wave functions are represented on the grid points. The dynamic polarizabilities may be calculated perturbatively by expanding the dipole moment in a power series of the external field strength or directly by integrating the real-time equations of motion under the time-varying external field. We describe the equations and computational techniques for the both methods. Besides calculating second-order and third-order hyperpolarizabilities, the method can be applied to photon-absorption cross sections, and we show examples of this application as well. We also present here for the first time calculations of the nonlinear polarizabilities using the real-time method.

Keywords: Time-dependent density-functional theory, real-space method, real-time method, polarizability, hyperpolarizability, response function method

PACS: 42.65.An, 42.65.Ky, 42.50.Hz, 31.15.Ew, 31.15.Fx, 02.70.Bf

1. Introduction

Optical properties of atoms and molecules are characterized by their linear and nonlinear polarizabilities. They reflect time-dependent dynamics of electrons under periodic external fields. Among numerous theoretical approaches developed to calculate polarizabilities, the time-dependent density-functional theory (TDDFT) has attracted broad interest and is expected to be quite practical to describe optical responses of large systems [1–8].

In the TDDFT, many-electron dynamics is described by the time-dependent Kohn-Sham equation, an effective single-particle Schrödinger equation in which electron-electron interactions are treated through a time-varying potential [9]. We have been developing and applying the real-space and real-time approaches for the dynamic polarizabilities based on the TDDFT [3,4,10–14]. In this real-space method, the kinetic operator in the Kohn-Sham is represented by a finite different approximation on a uniform Cartesian grid. Since the potential is usually local in the coordinate representation, the real-space method offers the economy of sparse matrix operations.

*Corresponding author. E-mail: iwata@cm.ph.tsukuba.ac.jp.

We have developed two distinct approaches to calculate linear and nonlinear polarizabilities in the uniform grid representation. One is the real-time method in which the time-dependent Kohn-Sham equation is solved explicitly in time domain [3]. This is especially useful for the calculations of linear polarizability. The other is the perturbative formalism [4,14]. In this method, the response of the system is calculated for a perturbation of a given frequency.

In this paper, we first give an overview of the real-space and real-time method. We then present two new results. One is the real-time computation of the nonlinear polarizabilities. Our previous application of the real-time method was limited to the calculation of the linear polarizability [3]. We here report for the first time the calculation of the nonlinear polarizabilities in the real-space and real-time method, taking high order harmonic generation of Ar atom as example. The other is the calculation of the two-photon absorption cross section. The two-photon absorption is related to the imaginary part of a certain third-order nonlinear polarizability. In Ref. [4], we have reported a real-space computational method of the molecular hyperpolarizabilities. It was, however, limited to the computation of the real part. We here report the calculation of the imaginary part of the hyperpolarizability. Results are presented for Ar atom and ethylene molecule.

2. Formalism

2.1. Definitions of polarizabilities

In this section, we summarize the fundamental quantities, the polarizabilities, which characterize linear and nonlinear optical responses of atoms and molecules [15]. We consider an external field of a superposition of monochromatic waves

$$\mathbf{E}(t) = \frac{1}{2}\sum_{\omega_i \geqslant 0} \left\{ \mathbf{E}_{\omega_i} e^{-i\omega_i t} + \mathbf{E}_{-\omega_i} e^{i\omega_i t} \right\}. \tag{1}$$

When the strength of the fields are moderate, the induced dipole moment can be expanded as the following power series.

$$\mathbf{p}(t) = \mathbf{p}^{(0)} + \mathbf{p}^{(1)}(t) + \mathbf{p}^{(2)}(t) + \mathbf{p}^{(3)}(t) + \cdots. \tag{2}$$

Each $\mathbf{p}^{(k)}(t)$ can be expressed as

$$\mathbf{p}^{(k)}(t) = \frac{1}{2}\sum_{\omega_\sigma \geqslant 0} \left\{ \mathbf{p}^{(k)}_{\omega_\sigma} e^{-i\omega_\sigma t} + \mathbf{p}^{(k)}_{-\omega_\sigma} e^{i\omega_\sigma t} \right\}, \tag{3}$$

where the Cartesian μ-component of $\mathbf{p}^{(k)}_{\omega_\sigma}$ is given by

$$\begin{aligned} \left(\mathbf{p}^{(k)}_{\omega_\sigma}\right)_\mu = \frac{1}{k!} \sum_{\alpha_1 \cdots \alpha_k} \sum_{\{\omega_1 \cdots \omega_k\}} & K(-\omega_\sigma; \omega_1, \cdots, \omega_k) \chi^{(k)}_{\mu\alpha_1\cdots\alpha_k}(-\omega_\sigma; \omega_1, \cdots, \omega_k) \\ & (\mathbf{E}_{\omega_1})_{\alpha_1} \cdots (\mathbf{E}_{\omega_k})_{\alpha_k}. \end{aligned} \tag{4}$$

The $\chi^{(k)}_{\mu\alpha_1\cdots\alpha_k}(-\omega_\sigma; \omega_1, \cdots, \omega_k)$ is the k-th order nonlinear polarizability tensor. The sum $\sum_{\{\omega_1\cdots\omega_k\}}$ is taken over all distinct sets of $\{\omega_1, \cdots, \omega_k\}$ whose sum is equal to ω_σ. $K(-\omega_\sigma; \omega_1, \cdots, \omega_k)$ is a

numerical factor given by $2^{l+m-k}p$ where p is the number of distinct permutations of $\{\omega_1, \cdots, \omega_k\}$, k is the order of nonlinearity, and m is the number of frequencies which are equal to zero. $l = 1$ if $\omega_\sigma = 0$ and $l = 0$ otherwise.

At present, a few of the lowest order polarizabilities (up to third order in usual) are the subjects of many theoretical and experimental studies, because they are related to the important physical phenomena, such as harmonic generations, Kerr effects, photoabsorptions, wave-mixings, and so on [15]. The nonlinear polarizabilities up to third order are often described by the special symbols, $\alpha(-\omega_1;\omega_1)$ for linear polarizability ($k = 1$), $\beta(-\omega_\sigma;\omega_1,\omega_2)$ for $k = 2$ and $\gamma(-\omega_\sigma;\omega_1,\omega_2,\omega_3)$ for $k = 3$ nonlinear polarizabilities. These symbols may also be used in this paper.

2.2. *Time-dependent density-functional theory*

The density-functional theory has been remarkably successful in describing electronic ground states and now plays a central role in the first-principle calculations of material properties. The TDDFT is an extension of the density-functional theory to describe the electronic dynamics induced by a time-varying external field [9,11]. The strategy to describe linear and nonlinear response properties in TDDFT is given below.

We consider a quantum system under the external potential $v^{\text{ext}}(\mathbf{r}, t)$. In the TDDFT, the time evolution of the density distribution $n(\mathbf{r}, t)$ is described by the time-dependent Kohn-Sham equation,

$$i\hbar\frac{\partial}{\partial t}\psi_i(\mathbf{r}, t) = \left\{h[n(t)] + v^{\text{ext}}(\mathbf{r}, t)\right\}\psi_i(\mathbf{r}, t), \tag{5}$$

$$h[n(t)] = -\frac{\hbar^2}{2m}\nabla^2 + V_{\text{ion}}(\mathbf{r}) + e^2\int d\mathbf{r}'\frac{n(\mathbf{r}', t)}{|\mathbf{r} - \mathbf{r}'|} + \mu_{xc}[n(t)], \tag{6}$$

$$n(\mathbf{r}, t) = \sum_{i\in occ}|\psi_i(\mathbf{r}, t)|^2, \tag{7}$$

where $\mu[n(t)]$ expresses the exchange-correlation potential.

The dipole field $\mathbf{E}(t)$ of Eq. (1) is expressed as the external potential,

$$v^{\text{ext}}(\mathbf{r}, t) = \frac{1}{2}\sum_{\omega_i \geqslant 0}\left\{v^{\text{ext}}_{\omega_i}(\mathbf{r})e^{-i\omega_i t} + v^{\text{ext}}_{-\omega_i}(\mathbf{r})e^{i\omega_i t}\right\}, \tag{8}$$

with

$$v^{\text{ext}}_{\omega_i}(\mathbf{r}) = e\mathbf{r}\mathbf{E}_{\omega_i}. \tag{9}$$

When the external field is not so strong, one can expand the density $n(\mathbf{r}, t)$ in a power series as,

$$n(\mathbf{r}, t) = n^{(0)}(\mathbf{r}) + n^{(1)}(\mathbf{r}, t) + n^{(2)}(\mathbf{r}, t) + n^{(3)}(\mathbf{r}, t) + \cdots. \tag{10}$$

Each $n^{(k)}(\mathbf{r}, t)$ can be expressed in a similar way to Eq. (3) where the general form of the dipole moment $\mathbf{p}^{(k)}(t)$ is given,

$$n^{(k)}(\mathbf{r}, t) = \frac{1}{2}\sum_{\omega_\sigma \geqslant 0}\left\{n^{(k)}_{\omega_\sigma}(\mathbf{r})e^{-i\omega_\sigma t} + n^{(k)}_{-\omega_\sigma}(\mathbf{r})e^{i\omega_\sigma t}\right\}, \tag{11}$$

with

$$n^{(k)}_{\omega_\sigma}(\mathbf{r}) = \frac{1}{k!} \sum_{\alpha_1 \cdots \alpha_k} \sum_{\{\omega_1 \cdots \omega_k\}} K(-\omega_\sigma; \omega_1, \cdots, \omega_k) n^{(k)}_{\alpha_1 \cdots \alpha_k}(\mathbf{r}| - \omega_\sigma; \omega_1, \cdots, \omega_k) \\ (\mathbf{E}_{\omega_1})_{\alpha_1} \cdots (\mathbf{E}_{\omega_k})_{\alpha_k}. \tag{12}$$

The k-th order nonlinear polarizability tensor can then be expressed in terms of the k-th order density as

$$\chi^{(k)}_{\mu\alpha_1 \cdots \alpha_n}(-\omega_\sigma; \omega_1, \cdots, \omega_k) = \int d\mathbf{r}(-er_\mu) n^{(k)}_{\alpha_1, \cdots, \alpha_k}(\mathbf{r}| - \omega_\sigma; \omega_1, \cdots, \omega_k). \tag{13}$$

In short, a k-th order polarizability can be obtained through the perturbative expansion of the time-dependent density Eq. (10), and pulling out a component of the density or its dipole moment which has the same order and the same Fourier component of the k-th order polarizability.

2.3. Perturbative formalism

We will consider two distinct approaches to calculate linear and nonlinear polarizabilities in TDDFT. One is the real-time method where the polarizabilities are calculated directly from the real-time evolution of the wave functions. The method is non-perturbative, namely the effects of the all orders of perturbation series are involved. However, one can pull out a few lowest order responses to the applied external potential of moderate intensity by sorting the Fourier components of the induced dipole moment. In this method, the polarizabilities can be obtained directly from the definitions given in the previous subsection and no further development of the formalism is required, in other words the working equation of the method is nothing but Eqs (5)–(7). The details of the method will be discussed in Section 4.

The other approach is the perturbative method which is more traditional one to calculate polarizabilities [1,2], however the working equations are quite different from the original time-dependent Kohn-Sham equation. The perturbative method for nonlinear response problems has been developed for atoms [2] and molecules [4]. We here briefly summarize the basic formalism and the working equations suitable for practical numerical calculations.

The basic quantities to be calculated in the perturbative formalism is the individual k-th order density of definite Fourier component $n^{(k)}_{\mu\alpha_1, \cdots, \alpha_n}(\mathbf{r}| - \omega_\sigma; \omega_1, \cdots, \omega_k)$. A perturbation expansion gives a hierarchy of equations which determine these densities order by order. The first-order equation is the linear response equation [1],

$$n^{(1)}_{\alpha_1}(\mathbf{r}| - \omega_\sigma; \omega_\sigma) = \int d\mathbf{r}_1 \chi^{(1)}_0(\mathbf{r}, \mathbf{r}_1; \omega_\sigma) h^{(1)}_{\alpha_1}(\mathbf{r}_1| - \omega_\sigma; \omega_\sigma), \tag{14}$$

$$h^{(1)}_{\alpha_1}(\mathbf{r}| - \omega_\sigma; \omega_\sigma) = \int d\mathbf{r}_1 \left\{ \frac{e^2}{|\mathbf{r} - \mathbf{r}_1|} + f_{xc}(\mathbf{r}, \mathbf{r}_1; \omega_\sigma) \right\} n^{(1)}_{\alpha_1}(\mathbf{r}_1| - \omega_\sigma; \omega_\sigma) + er_{\alpha_1}, \tag{15}$$

where ω_σ is one of the frequency of the external field $\{\pm\omega_i\}$. The (independent-particle version) frequency-domain density-density response function $\chi^{(1)}_0(\mathbf{r}, \mathbf{r}'; \omega_\sigma)$ and exchange-correlation kernel

$f_{xc}(\mathbf{r},\mathbf{r}';\omega_\sigma)$ which is a functional derivative of the exchange-correlation potential with respect to the density, are introduced. The explicit expression of $\chi_0^{(1)}(\mathbf{r},\mathbf{r}';\omega_\sigma)$ is given by [1,2],

$$\chi_0^{(1)}(\mathbf{r},\mathbf{r}';\omega_\sigma) = \sum_i^{occ.} \left[\phi_i^*(\mathbf{r}) G^{(+)}(\mathbf{r},\mathbf{r}';\varepsilon_i + \hbar\omega_\sigma)\phi_i(\mathbf{r}') + \phi_i^*(\mathbf{r}') G^{(-)}(\mathbf{r}',\mathbf{r};\varepsilon_i - \hbar\omega_\sigma)\phi_i(\mathbf{r}) \right], \quad (16)$$

where $G^{(\pm)}(\mathbf{r},\mathbf{r}';\omega_\sigma)$ is the (frequency-domain) single-particle Green function [1,14],

$$G^{(\pm)}(\mathbf{r},\mathbf{r}';E) = \sum_\mu \frac{\phi_\mu(\mathbf{r})\phi_\mu^*(\mathbf{r}')}{E - \varepsilon_\mu \pm i\eta}, \quad (17)$$

where η is a positive infinitesimal. Equations (14)–(16) have been solved directly with explicit construction of the response function for spherical systems such as atoms [1] or jellium clusters [16,17]. For systems without spherical symmetry, however, the integral Eq. (14) should be recasted into the equivalent differential equation,

$$n_{\alpha_1}^{(1)}(\mathbf{r}|-\omega_\sigma;\omega_\sigma) = \sum_{i\in occ.} \left\{ \phi_i^*(\mathbf{r})\psi_{i,\alpha_1}^{(1)}(\mathbf{r}|-\omega_\sigma;\omega_\sigma) + \phi_i(\mathbf{r})\psi_{i,\alpha_1}^{(1)*}(\mathbf{r}|\omega_\sigma;-\omega_\sigma) \right\}, \quad (18)$$

where $\psi_{i,\alpha_1}^{(1)}(\mathbf{r}|-\omega_\sigma;\omega_\sigma)$, $\psi_{i,\alpha_1}^{(1)*}(\mathbf{r}|\omega_\sigma;-\omega_\sigma)$ satisfy the following differential equations,

$$(\varepsilon_i + \hbar\omega_\sigma - h[n])\psi_{i,\alpha_1}^{(1)}(\mathbf{r}|-\omega_\sigma;\omega_\sigma) = h_{\alpha_1}^{(1)}(\mathbf{r}|-\omega_\sigma;\omega_\sigma)\phi_i(\mathbf{r}), \quad (19)$$

$$(\varepsilon_i - \hbar\omega_\sigma - h[n])\psi_{i,\alpha_1}^{(1)}(\mathbf{r}|\omega_\sigma;-\omega_\sigma) = h_{\alpha_1}^{(1)*}(\mathbf{r}|-\omega_\sigma;\omega_\sigma)\phi_i(\mathbf{r}). \quad (20)$$

These are known as the Sternheimer equations. We call the present differential form of the linear response problem as the modified Sternheimer method [18].

The second- and the third-order equations can be developed systematically. The second-order equations are

$$n_{\alpha_1\alpha_2}^{(2)}(\mathbf{r}|-\omega_\sigma;\omega_1,\omega_2) = \sum_{i\in occ.} \left\{ \phi_i^*(\mathbf{r})\psi_{i,\alpha_1\alpha_2}^{(2)}(\mathbf{r}|-\omega_\sigma;\omega_1,\omega_2) + \phi_i(\mathbf{r})\psi_{i,\alpha_1\alpha_2}^{(2)*}(\mathbf{r}|\omega_\sigma;-\omega_1,-\omega_2) + \hat{\mathbf{S}}_{12}\left[\psi_{i,\alpha_1}^{(1)*}(\mathbf{r}|\omega_1;-\omega_1)\psi_{i,\alpha_2}^{(1)}(\mathbf{r}|-\omega_2;\omega_2)\right] \right\}, \quad (21)$$

$$(\varepsilon_i + \hbar\omega_\sigma - h[n])\psi_{i,\alpha_1\alpha_2}^{(2)}(\mathbf{r}|-\omega_\sigma;\omega_1,\omega_2) = h_{\alpha_1\alpha_2}^{(2)}(\mathbf{r}|-\omega_\sigma;\omega_1,\omega_2)\phi_i(\mathbf{r}) + \hat{\mathbf{S}}_{12}\left[h_{\alpha_1}^{(1)}(\mathbf{r}|-\omega_1;\omega_1)\psi_{i,\alpha_2}^{(1)}(\mathbf{r}|-\omega_2;\omega_2)\right], \quad (22)$$

$$(\varepsilon_i - \hbar\omega_\sigma - h[n])\psi_{i,\alpha_1\alpha_2}^{(2)}(\mathbf{r}|\omega_\sigma;-\omega_1,-\omega_2) = h_{\alpha_1\alpha_2}^{(2)}(\mathbf{r}|\omega_\sigma;-\omega_1,-\omega_2)\phi_i^*(\mathbf{r}) + \hat{\mathbf{S}}_{12}\left[h_{\alpha_1}^{(1)}(\mathbf{r}|\omega_1;-\omega_1)\psi_{i,\alpha_2}^{(1)*}(\mathbf{r}|\omega_2;-\omega_2)\right], \quad (23)$$

where $\hat{\mathbf{S}}_{12}$ indicates that the summation should be taken over all the possible permutations of the indices $\{1,2\}$. $h^{(2)}_{\alpha_1\alpha_2}(\mathbf{r}|-\omega_\sigma;\omega_1,\omega_2)$ include the second- and first-order densities as

$$h^{(2)}_{\alpha_1\alpha_2}(\mathbf{r}|-\omega_\sigma;\omega_1,\omega_2)=\int d\mathbf{r}_1\left\{\frac{e^2}{|\mathbf{r}-\mathbf{r}_1|}+f_{xc}(\mathbf{r},\mathbf{r}_1;\omega_\sigma)\right\}n^{(2)}_{\alpha_1\alpha_2}(\mathbf{r}_1|-\omega_\sigma;\omega_1,\omega_2)$$
$$+\int d\mathbf{r}_1\int d\mathbf{r}_2\; g_{xc}(\mathbf{r},\mathbf{r}_1,\mathbf{r}_2;\omega_1,\omega_2)n^{(1)}_{\alpha_1}(\mathbf{r}_1|-\omega_1;\omega_1)n^{(1)}_{\alpha_2}(\mathbf{r}_2|-\omega_2;\omega_2), \tag{24}$$

where $g_{xc}(\mathbf{r},\mathbf{r}_1,\mathbf{r}_2;\omega_1,\omega_2)$ is the second-order exchange-correlation kernel which is a second functional derivative of the exchange-correlation potential with respect to the density.

The third-order equations are

$$n^{(3)}_{\alpha_1\alpha_2\alpha_3}(\mathbf{r}|-\omega_\sigma;\omega_1,\omega_2,\omega_3)=\sum_{i\in occ.}\left\{\phi^*_i(\mathbf{r})\psi^{(3)}_{i,\alpha_1\alpha_2\alpha_3}(\mathbf{r}|-\omega_\sigma;\omega_1,\omega_2,\omega_3)+\phi_i(\mathbf{r})\psi^{(3)*}_{i,\alpha_1\alpha_2\alpha_3}\right.$$
$$(\mathbf{r}|\omega_\sigma;-\omega_1,-\omega_2,-\omega_3)+\hat{\mathbf{S}}_{123}\left[\psi^{(1)*}_{i,\alpha_1}(\mathbf{r}|\omega_1;-\omega_1)\psi^{(2)}_{i,\alpha_2\alpha_3}(\mathbf{r}|-\omega_2-\omega_3;\omega_2,\omega_3)\right] \tag{25}$$
$$\left.+\hat{\mathbf{S}}_{123}\left[\psi^{(1)}_{i,\alpha_1}(\mathbf{r}|-\omega_1;\omega_1)\psi^{(2)*}_{i,\alpha_2\alpha_3}(\mathbf{r}|\omega_2+\omega_3;-\omega_2,-\omega_3)\right]\right\},$$

$$(\varepsilon_i+\hbar\omega_\sigma-h[n])\psi^{(3)}_{i,\alpha_1\alpha_2\alpha_3}(\mathbf{r}|-\omega_\sigma;\omega_1,\omega_2,\omega_3)=h^{(3)}_{\alpha_1\alpha_2\alpha_3}(\mathbf{r}|-\omega_\sigma;\omega_1,\omega_2,\omega_3)\phi_i(\mathbf{r})$$
$$+\hat{\mathbf{S}}_{123}\left[h^{(1)}_{\alpha_1}(\mathbf{r}|-\omega_1;\omega_1)\psi^{(2)}_{i,\alpha_2\alpha_3}(\mathbf{r}|-\omega_2-\omega_3;\omega_2,\omega_3)\right] \tag{26}$$
$$+\hat{\mathbf{S}}_{123}\left[h^{(2)}_{\alpha_2\alpha_3}(\mathbf{r}|-\omega_2-\omega_3;\omega_2,\omega_3)\psi^{(1)}_{i,\alpha_1}(\mathbf{r}|-\omega_1;\omega_1)\right],$$

$$(\varepsilon_i-\hbar\omega_\sigma-h[n])\psi^{(3)}_{i,\alpha_1\alpha_2\alpha_3}(\mathbf{r}|\omega_\sigma;-\omega_1,-\omega_2,-\omega_3)=h^{(3)}_{\alpha_1\alpha_2\alpha_3}(\mathbf{r}|\omega_\sigma;-\omega_1,-\omega_2,-\omega_3)\phi^*_i(\mathbf{r})$$
$$+\hat{\mathbf{S}}_{123}\left[h^{(1)}_{\alpha_1}(\mathbf{r}|-\omega_1;\omega_1)\psi^{(2)*}_{i,\alpha_2\alpha_3}(\mathbf{r}|\omega_2+\omega_3;-\omega_2,-\omega_3)\right] \tag{27}$$
$$+\hat{\mathbf{S}}_{123}\left[h^{(2)}_{\alpha_2\alpha_3}(\mathbf{r}|-\omega_2-\omega_3;\omega_2,\omega_3)\psi^{(1)*}_{i,\alpha_1}(\mathbf{r}|\omega_1;-\omega_1)\right],$$

where $\hat{\mathbf{S}}_{123}$ indicates that the summation should be taken over all the possible permutations of the indices $\{1,2,3\}$. $h^{(3)}_{\alpha_1\alpha_2\alpha_3}(\mathbf{r}|-\omega_\sigma;\omega_1,\omega_2,\omega_3)$ includes the first-, second- and third-order densities as

$$h^{(3)}_{\alpha_1\alpha_2\alpha_3}(\mathbf{r}|-\omega_\sigma;\omega_1,\omega_2,\omega_3)=\int d\mathbf{r}_1\left\{\frac{e^2}{|\mathbf{r}-\mathbf{r}_1|}+f_{xc}(\mathbf{r},\mathbf{r}_1;\omega_\sigma)\right\}n^{(3)}_{\alpha_1\alpha_2\alpha_3}(\mathbf{r}_1|-\omega_\sigma;\omega_1,\omega_2,\omega_3)$$
$$+\int d\mathbf{r}_1\int d\mathbf{r}_2\; g_{xc}(\mathbf{r},\mathbf{r}_1,\mathbf{r}_2;\omega_1,\omega_2+\omega_3)n^{(1)}_{\alpha_1}(\mathbf{r}_1|-\omega_1;\omega_1)n^{(2)}_{\alpha_2\alpha_3}(\mathbf{r}_2|-\omega_2-\omega_3;\omega_2,\omega_3)$$
$$+\int d\mathbf{r}_1\int d\mathbf{r}_2\; g_{xc}(\mathbf{r},\mathbf{r}_1,\mathbf{r}_2;\omega_2,\omega_3+\omega_1)n^{(1)}_{\alpha_2}(\mathbf{r}_1|-\omega_2;\omega_2)n^{(2)}_{\alpha_3\alpha_1}(\mathbf{r}_2|-\omega_3-\omega_1;\omega_3,\omega_1) \tag{28}$$
$$+\int d\mathbf{r}_1\int d\mathbf{r}_2\; g_{xc}(\mathbf{r},\mathbf{r}_1,\mathbf{r}_2;\omega_3,\omega_1+\omega_2)n^{(1)}_{\alpha_3}(\mathbf{r}_1|-\omega_3;\omega_3)n^{(2)}_{\alpha_1\alpha_2}(\mathbf{r}_2|-\omega_1-\omega_2;\omega_1,\omega_2)$$

$$+\int d\mathbf{r}_1 \int d\mathbf{r}_2 \int d\mathbf{r}_3\; h_{xc}(\mathbf{r},\mathbf{r}_1,\mathbf{r}_2,\mathbf{r}_3;\omega_1,\omega_2,\omega_3)$$
$$\times n^{(1)}_{\alpha_1}(\mathbf{r}_1|-\omega_1;\omega_1) n^{(1)}_{\alpha_2}(\mathbf{r}_2|-\omega_2;\omega_2) n^{(1)}_{\alpha_3}(\mathbf{r}_3|-\omega_3;\omega_3).$$

where $h_{xc}(\mathbf{r},\mathbf{r}_1,\mathbf{r}_2,\mathbf{r}_3;\omega_1,\omega_2,\omega_3)$ is the third-order exchange-correlation kernel which is a third functional derivative of the exchange-correlation potential with respect to the density.

In the TDDFT, exchange and correlation effects are included in the exchange-correlation potential μ_{xc} and kernels f_{xc}, g_{xc}, and h_{xc}. In most calculations, the exchange-correlation potential which is local in time (adiabatic approximation) and in space (local-density approximation) is employed. This is sometimes called the adiabatic local-density approximation (ALDA). In the ALDA, the exchange-correlation potential and kernels are given as follows,

$$f_{xc}(\mathbf{r},\mathbf{r}_1;\omega) = \frac{d\mu_{xc}}{dn}\delta(\mathbf{r}-\mathbf{r}_1), \tag{29}$$

$$g_{xc}(\mathbf{r},\mathbf{r}_1,\mathbf{r}_2;\omega_1,\omega_2) = \frac{d^2\mu_{xc}}{dn^2}\delta(\mathbf{r}-\mathbf{r}_1)\delta(\mathbf{r}_1-\mathbf{r}_2), \tag{30}$$

$$h_{xc}(\mathbf{r},\mathbf{r}_1,\mathbf{r}_2,\mathbf{r}_3;\omega_1,\omega_2,\omega_3) = \frac{d^3\mu_{xc}}{dn^3}\delta(\mathbf{r}-\mathbf{r}_1)\delta(\mathbf{r}_1-\mathbf{r}_2)\delta(\mathbf{r}_2-\mathbf{r}_3). \tag{31}$$

3. Real-space computational method

3.1. Hamiltonian

Our method utilizes the uniform grid representation in the three-dimensional Cartesian coordinates. The uniform grid representation is convenient in the Kohn-Sham theory where the self-consistent potential is almost local in the coordinate representation. It is also advantageous to describe isolated molecules since the boundary condition can be imposed naturally. The uniform grid representation is also considered to be suitable for the parallel computation, although our present calculations are achieved with a single processor.

In the uniform grid representation, one cannot explicitly treat core electrons, since the description of core electrons requires very fine grid spacing. Instead, one employs pseudopotential which describes interaction between valence electrons and ion. Among existing methods to construct pseudopotentials, we employ the norm-conserving pseudpotential with a prescription proposed by Troullier and Martins [19]. The norm-conserving pseudopotential is nonlocal, dependent on the relative angular momentum between the electron and ion. Denoting the potential for l-th partial wave as $V_l^{\rm ion}(r)$, the pseudopotential is expressed as

$$V^{\rm ion}(\mathbf{r},\mathbf{r}') = \sum_{\rm lm} V_l^{\rm ion}(r)\frac{\delta(r-r')}{rr'}Y^*_{\rm lm}(\hat{r})Y_{\rm lm}(\hat{r}') \tag{32}$$

This form of potential, local in the radial distance r and nonlocal in the angular variable $\hat{r}$, is not convenient in the uniform grid representation. We instead employ separable approximation to the

potential which is known as the Kleinman-Bylander procedure [20],

$$V_{KB}^{\rm ion}({\bf r},{\bf r}') = \sum_{lm} \frac{V_l^{\rm ion}(r)\phi_{lm}({\bf r})V_l^{\rm ion}(r')\phi_{lm}^*({\bf r}')}{\langle\phi_{lm}|V_l^{\rm ion}|\phi_{lm}\rangle}, \tag{33}$$

where $\phi_{lm}({\bf r})$ is the valence orbital wave functions of an atom with angular momentum lm, constructed with the pseudopotential $V_l^{\rm ion}(r)$.

In the uniform grid representation, it is known that, for a fixed grid spacing, one can obtain more accurate results by employing higher-order finite-difference formula to deal with the kinetic energy operator [21]. We will employ nine-point finite-difference formula.

3.2. Ground state construction

For response calculations, one first need to construct Kohn-Sham ground state. This step is achieved as follows. We first prepare an initial guess for the Kohn-Sham orbitals ϕ_i and the density. For a given density $n({\bf r})$, the Kohn-Sham Hamiltonian $h[n]$ is constructed. With this Hamiltonian, we improve the orbital wave functions employing a conjugate gradient method. At this step, the number of iterations of the conjugate gradient procedure is set to be rather small, usually 3 or 4. The orbital wave functions are then orthonormalized by the Schmidt procedure. The density and the Kohn-Sham Hamiltonian is then updated. This iterative procedure is continued until convergence. Although this procedure to obtain the ground state is not very sophisticated, it works robustly.

In constructing the Kohn-Sham Hamiltonian from the density, one need to calculate the Hartree potential. We calculate it by solving the Poisson equation employing the conjugate gradient method. To start the procedure, the boundary condition for the Hartree potential is required. We make use of the multipole expansion of the electron density around each atom to prepare the boundary condition.

3.3. Time evolution

The real-time evolution of the wave function is achieved by the Taylor expansion of the time evolution operator [3,22]. For a short period Δt, we ignore the change of the Hamiltonian $h[n(t)]$ in time. The wave function at $t+\Delta t$, $\psi(t+\Delta t)$, is obtained from the wave function at t, $\psi(t)$, by

$$\psi_i(t+\Delta t) \simeq \exp\left[-\frac{i}{\hbar}h[n(t)]\Delta t\right]\psi_i(t) \simeq \sum_k^{N_{max}} \frac{1}{k!}\left(\frac{-i\Delta t}{\hbar}h[n(t)]\right)^n \psi_i(t) \tag{34}$$

To achieve stable time evolution, one should choose N_{max} and Δt so that no eigenvalue of the approximated operator has a modulus greater than unity [11]. The maximum eigenvalue ε_{max} of $h[n(t)]$ is essentially determined by the kinetic energy operator; it may be estimated from the grid spacing Δx as $\varepsilon_{max} \sim 3(\hbar^2/2m)(\pi/\Delta x)^2$. We use the choice $N_{max} = 4$, for which the stability condition is

$$\Delta t \leqslant \sqrt{8}\frac{\hbar}{\varepsilon_{max}}. \tag{35}$$

In the Taylor expansion method, the time evolution is not exactly unitary. In practice, however, we found that the violation of the unitarity has negligible effect on the observables calculated here. We also find that the orthogonality of the wave functions ψ_i is preserved in the time evolution without requiring orthonormalization in the time evolution.

3.4. *Perturbative calculation*

In the perturbative method described in Section 2.3, the k-th order density $n^{(k)}(\mathbf{r})$ can be obtained by solving the Sternheimer equations order by order. We here explain this procedure in more detail. Looking carefully at the structure of the equations Eqs (18)–(29), the k-th order density $n^{(k)}_{\alpha_1\cdots\alpha_k}(\mathbf{r}|-\omega_\sigma;\omega_1\cdots\omega_k)$ which we simply denote $n^{(k)}(\mathbf{r})$ below satisfies the equation which has the same structure as the linear response Eq. (14).

$$n^{(k)}(\mathbf{r}) = \int d\mathbf{r}_1 \chi_0^{(1)}(\mathbf{r},\mathbf{r}_1;\omega_\sigma) \int d\mathbf{r}_2 \left\{ \frac{e^2}{|\mathbf{r}_1-\mathbf{r}_2|} + f_{xc}(\mathbf{r}_1)\delta(\mathbf{r}_1-\mathbf{r}_2) \right\} n^{(k)}(\mathbf{r}_2) + n_0^{(k)}(\mathbf{r}), \quad (36)$$

where $n_0^{(k)}(\mathbf{r})$ indicates a term which includes quantities of lower orders ($\leqslant k-1$). This equation for an unknown function $n^{(k)}(\mathbf{r})$ can be regarded as a linear algebraic equation in the uniform grid representation. Since the coefficient matrix of the equation is not Hermitian, we employ the generalized-conjugate-residual method which is an extension of the well-known conjugate-gradient method for non-Hermitian problems [4,23].

In practice, integrals in Eq. (36) are treated by converting them into equivalent differential equations, going back to the original differential form given by Eqs (18)–(29). In calculating $h^{(k)}_{\alpha_1\cdots\alpha_k}(\mathbf{r})$, the integral involving Coulomb potential is converted into the Poisson equation, and it is solved by the conjugate gradient method. The Sternheimer equations are the linear algebraic equation with a symmetric coefficient matrix after discretization. This is solved again by the conjugate gradient method for real frequencies. For complex frequencies, the coefficient matrix is not Hermitian. We found the bi-conjugate-gradient method works well for this case, even when the frequency is near the resonance energy of the system.

In solving the Sternheimer equations, it is important to treat the component of occupied orbitals separately to accelerate the convergence. For example, Eq. (19) is solved first in the space orthogonal to the occupied orbitals. Namely, we solve

$$(\varepsilon_i + \hbar\omega_\sigma - h[n])\tilde{\psi}_i^{(1)}(\mathbf{r}) = h^{(1)}(\mathbf{r})\phi_i(\mathbf{r}) - \sum_{j\in occ.} \phi_j(\mathbf{r})\langle\phi_j|h^{(1)}|\phi_i\rangle. \quad (37)$$

The occupied orbital components are then added.

$$\psi_i^{(1)}(\mathbf{r}) = \tilde{\psi}_i^{(1)}(\mathbf{r}) + \sum_{j\in occ.} \frac{1}{\varepsilon_i - \varepsilon_j + \hbar\omega_\sigma} \phi_j(\mathbf{r})\langle\phi_j|h^{(1)}|\phi_i\rangle. \quad (38)$$

This procedure is always applied when we solve the Sternheimer equations.

4. Real-time method

In this section, we discuss a real-time computational method for polarizabilities. The real-time method works most efficiently for the calculations of linear polarizabilities, and has been applied to calculating photoabsorption of various systems [3,10]. We first briefly explain it.

4.1. Instantaneous external field

We consider a system under a weak external electric field $E(t)$ of any time profile. We introduce the linear polarizability function in time domain, $\alpha(t)$. This function relates the external electric field $E(t)$ with the induced dipole moment $p(t)$ by

$$p(t) = \int_{-\infty}^{t} dt' \alpha(t - t')E(t'). \tag{39}$$

The frequency-dependent polarizability is obtained from $\alpha(t)$ by the Fourier transformation,

$$\alpha(\omega) = \int_{0}^{+\infty} dt e^{i\omega t} \alpha(t). \tag{40}$$

The lower limit of the integral reflects the causality condition.

If Eq. (39) can be inverted, one may employ any external field $E(t)$ to obtain $\alpha(t)$. The simplest choice for $E(t)$ is the instantaneous external field, $eE(t) = k\delta(t)$, where k is a small parameter to ensure the linear response. Right after this instantaneous dipole field, all electrons in the system receive impulsive force. Taking the direction of this field as z-axis, all the orbital wave functions are multiplied by a plane wave, $\phi_i(\mathbf{r}) \to e^{ikz}\phi_i(\mathbf{r})$. The time-dependent Kohn-Sham equation is then solved with this initial wave function and without any external potential. The dipole polarizability in time is obtainable from the dipole moment,

$$\alpha(t) = -\frac{e^2}{k} \int d\mathbf{r} z n(\mathbf{r}, t). \tag{41}$$

In this real-time method with the instantanous external field, one can obtain frequency-dependent polarizability $\alpha(\omega)$ of full spectral region from a single time evolution calculation. A finite time period of the time evolution limits the resolution of the obtained frequency-dependent polarizability, which we denote ΔE. It is related to the length of the time evolution, T, by the uncertainty relation, $\Delta E = 2\pi/T$.

This real-time method for the linear polarizability has been successfully applied for various molecules and clusters [3,10–13]. The usefulness of the instantaneous external field is, however, limited to the calculation of the linear polarizability.

4.2. Sinusoidal external field

We here propose a new real-time approach which can be applied to the nonlinear polarizabilities as well as the linear one. This is an extension of the finite field approach for frequency-independent responses [24]. In this approach, we apply an external field consisting, in general, of several sinusoidal time-dependences. For simplicity, we consider a case of calculating high harmonic generation where a monochromatic external field is applied to a system. We apply the dipole external field of the following form,

$$V_{\text{ext}}(t) = f(t)kz \cos \omega t, \tag{42}$$

where the function $f(t)$ describes the time profile of the external field. We employ a function $f(t)$ that increases smoothly from zero to unity to simulate the adiabatic switching. In the adiabatic limit,

we expect the electrons to respond with the frequency equal to the external one and its harmonics. In practicical calculations, we will employ the function

$$f(t) = \begin{cases} 0 & t < 0 \\ \frac{1}{2}\left(1 - \cos \pi \frac{t}{\tau}\right) & 0 < t < \tau \\ 1 & \tau < t \end{cases}, \tag{43}$$

where the parameter τ controlls the adiabaticity.

If the adiabaticity is well satisfied, the electrons in the system oscillates periodically with the period of the external field, $T = 2\pi/\omega$ at $t > \tau$. The dipole moment $d(t) = \int dr z n(\mathbf{r}, t)$ should be periodic as well, $d(t + T) = d(t)$. If we ignore the nonlinear polarizabilities higher than third order, the dipole moment can be expressed

$$d(t) = (d^{(0)} + d_0^{(2)}) + (d_\omega^{(1)} + d_\omega^{(3)}) \cos \omega t + d_{2\omega}^{(2)} \cos 2\omega t + d_{3\omega}^{(3)} \cos 3\omega t. \tag{44}$$

We introduce the Fourier components of the dipole moments as

$$d_n = \frac{2}{T} \int_{mT}^{(m+1)T} dt e^{in\omega t} d(t), \tag{45}$$

which should be independent of which cycle m is chosen, provided it is in the domain where $f = 1$. The linear and nonlinear polarizabilities can be expressed with these Fourier components as

$$\alpha_{zz}(-\omega; \omega) = -\frac{e^2}{k} d_1, \tag{46}$$

$$\beta_{zzz}(-2\omega; \omega\omega) = -\frac{4e^3}{k^2} d_2, \tag{47}$$

$$\gamma_{zzzz}(-3\omega; \omega\omega\omega) = -\frac{24e^4}{k^3} d_3. \tag{48}$$

These relations allow us to calculate frequency-dependent linear and nonlinear polarizabilities of high harmonic generation from the real-time calculation. We should note that these relationships hold on condition that the parameter k, which controlls the strength of the external field, is small enough so that the higher order effects are negligible. On the other hand, the parameter k should be taken sufficiently large to avoid rounding error.

4.3. Example: Ar atom

As an example of the real-time method, we calculate here the linear and nonlinear polarizabilities of Ar atom. We apply an external dipole field of time profile given by Eqs (42) and (43) with the parameters, $\hbar\omega = 1.175$ eV and $\tau = 2T$. The strength of the external field k is varied in the range $0.5 \sim 1.5$ eV/Å. We take a grid points inside a sphere of 6 Å with grid spacing 0.3 Å. We employ the exchange-correlation potential and kernels of Perdew and Zunger [25] in the Kohn-Sham operator.

The linear and nonlinear polarizabilities of Ar atom have been reported in Ref. [4] employing the modified Sternheimer method which was explained in Section 2.3. The linear polarizability, $\alpha(\omega) = 12.2$ a.u., and the hyperpolarizability of third harmonic generation, $\gamma(-3\omega; \omega, \omega, \omega) = 2270$ a.u.

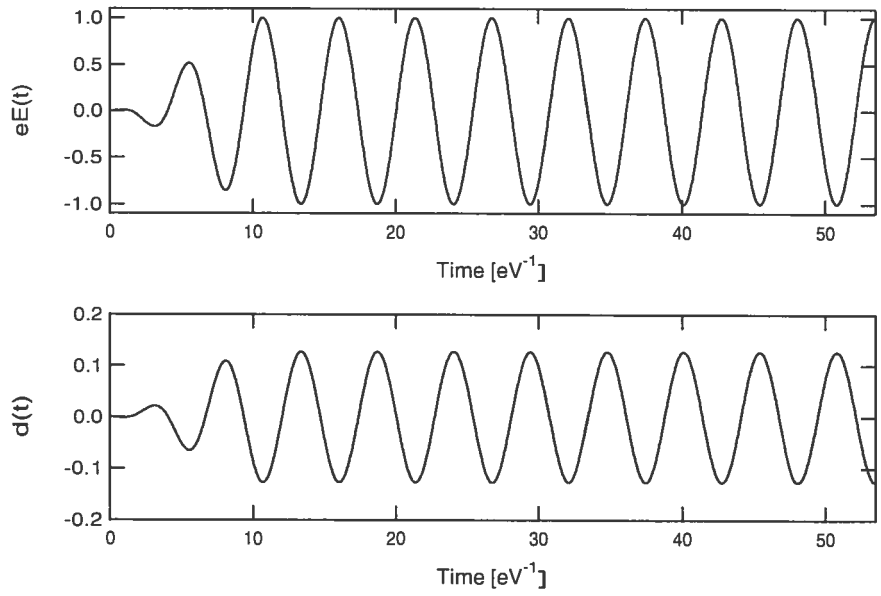

Fig. 1. Time profile of the external field $eE(t)$ and dipole moment $d(t)$. The intensity parameter k is set at 1 [eV/Å].

We show in Fig. 1 the time-dependence of the external field $eE(t)$ (upper panel) in eV/Å, and the induced dipole moment $d(t)$ (lower panel) in Å for the case of $k = 1.0$ eV/Å. It is apparent from the figure that the dipole moment closely follows the instantaneous electric field. Taking the Fourier transform of the computed $d(t)$ in the interval $[mT, (m+1)T]$ with $m = 2$, we can express $d(t)$ as the Fourier series

$$d(t) = -0.127 \cos \omega t - 0.000395 \cos 3\omega t + \cdots \tag{49}$$

The neglected terms in the series, $\cos n\omega t$ with even n, the higher harmonics $n \geqslant 5$, and terms proportional to $\sin n\omega t$, are small.

From the coefficient of $\cos \omega t$ and using Eq. (46), we can extract a value of 1.83 Å^3 for ordinary polarizability. This value is close to the polarizability $\alpha(\omega) = 12.2$ a.u. $\simeq 1.81$ Å^3 obtained by the modified Sternheimer method. The coefficient of $\cos 3\omega t$ represents the third harmonic generation. We found the coefficient of $\cos 2\omega t$ is very small, less than 10^{-6}; in principle it vanishes by symmetry and its numerical size gives an indication of the numerical precision of the calculation.

We next calculate the dipole polarizability $\alpha(\omega)$ as a function of field strength, using Eq. (46). We take the same adiabatic turn-on function f as in the previous paragraph. The calculated dipole polarizabilities do not depend much on the time period specified by m, but depend on k value. We take an average over m values in the range $2 \leqslant m \leqslant 10$ and show results in Fig. 2 as a function of the square of the strength parameter, k^2. The imaginary part of the calculated dipole polarizability is negligible.

We should note that, from Eq. (44), the coefficient of $\cos \omega t$ includes a contribution from the third order as well as the linear polarizability. This effect is seen in Fig. 3 as a linear dependence of the linear polarizability as a function of k^2. The polarizability extrapolated to $k \to 0$ coincides well with the calculated value $\alpha(\omega) = 12.2$ a.u. in the modified Sternheimer method.

We next turn to the hyperpolarizability of third harmonic generation, $\gamma(-3\omega; \omega, \omega, \omega)$. The hyperpolarizability is calculated according to Eq. (48) and the average is taken over the period $[2T, 10T]$, as in

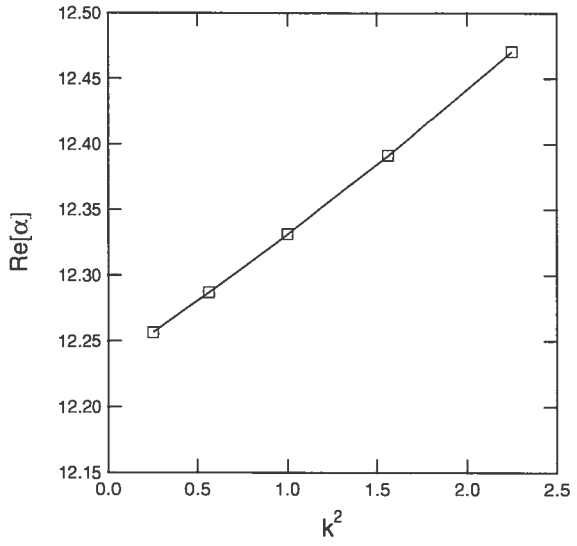

Fig. 2. Linear polarizability $\alpha(\omega)$ in a.u. is plotted against the square of the external field strength parameter, k^2.

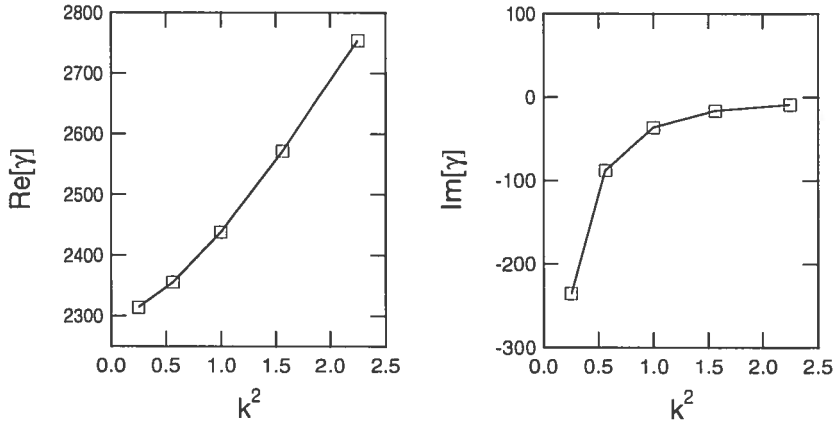

Fig. 3. Second hyperpolarizability of high order harmonics $\gamma(-3\omega;\omega,\omega,\omega)$ in a.u. is plotted against the square of the external field strength parameter, k^2. Real part (left-hand panel) and imaginary part (right-hand panel) are shown.

the case of the linear polarizability. The real and the imaginary part of the hyperpolarizability are plotted in Fig. 3 against k^2.

The hyperpolarizability calculated with the modified Sternheimer method is 2270 a.u. This is close to the value in the present real-time method taking a small k limit. There are, however, two problems which are not yet resolved. First the Re[γ] does not show quadratic dependence on k, although fifth order effect is expected to appear as the quadratic dependence in the present finite field calculation. Second, there appears substantial imaginary part when we make calculations with small k value. The hyperpolarizability should be real since $3\hbar\omega = 3.525$ eV is well below the ionization threshold. We cannot explain the origin of these problems, although, of course, we imagine the rounding errors at small k calculation could be a candidate of the possible origins.

Summarizing this section, we have proposed a new computational method for the frequency-dependent

linear and nonlinear polarizabilities. The most attractive feature of the present method is that it does not require any perturbative expansion. The polarizabilities are obtainable directly from the real-time calculation which requires rather small addition in the computational programming. Since the perturbative method requires development of lengthy formula and coding as shown in Section 2.3, this is a significant advantage of the present real-time method. Of course, the present real-time calculation can readily be applicable to the electron dynamics under the intense short pulse laser. In fact, the TDDFT has been extensively applied to the phenomena related to the strong laser field such as the high harmonic generation and ionization processes [9,26].

5. Two-photon absorption cross sections

In this section, we present results of the TDDFT calculation for hyperpolarizability in the complex energy plane. The imaginary part of the second hyperpolarizability $\gamma(-\omega;-\omega,\omega,\omega)$ provides two-photon absorption (TPA) cross section of the system. To our knowledge, this is a first attempt to calculate TPA in the TDDFT. When the frequency of the external field coincides with half of the excitation energies, the TPA takes place. In addition, the real-part of the hyperpolarizability shows divergent behavior at the frequencies. This enhanced hyperpolarizabilities at resonant frequency region are of technological interests. We will show that, employing the modified Sternheimer method explained in Section 2.3, the TPA and the resonant enhancement in the hyperpolarizability can be calculated stably. We show results taking Ar atom and ethylene molecule as examples.

5.1. Ar atom

We first show the TPA cross section of Ar atom. In order to get the information on the imaginary part of the hyperpolarizability, we introduce small imaginary component in the frequency and replace all the frequency arguments in the Sternheimer equations as

$$\hbar\omega \rightarrow \hbar\omega + i\eta \tag{50}$$

The perturbative calculaitons are done order by order according to the procedure explained in Sections 2.3 and 3.4. The small positive parameter η is chosen as $\eta = 0.1$ eV in the practical calculations. The uniform grid points inside a sphere of 5 Å with the grid spacing of 0.3 Å is employed. We use the LB94 exchange-correlation potential [27] in the ground state construction. The LB94 potential includes gradient correction which describes asymptotic $1/r$ behavior of the potential correctly. The adiabatic local-density approximation is assumed for the exchange-correlation kernels in the response calculations.

In Fig. 4, we show results of two calculations for the imaginary part of the hyperpolarizability $\gamma(-\omega;-\omega,\omega,\omega)$ varying $\hbar\omega$. The TDDFT calculation is shown by the solid curve and the response calculation in the independent-particle approximation (IPA) is shown by the dashed curve. The IPA implies that the induced field is ignored, namely the k-th order density is calculated by the k-th order density-density response function as

$$n^{(k)IPA}_{\alpha_1,\cdots,\alpha_k}(\mathbf{r}|-\omega_\sigma;\omega_1,\cdots,\omega_k) = \int d\mathbf{r}_1\cdots d\mathbf{r}_k \chi_0^{(k)}(\mathbf{r},\mathbf{r}_1,\cdots,\mathbf{r}_k;\omega_1,\cdots,\omega_k)(e\mathbf{r}_1)_{\alpha_1}\cdots(e\mathbf{r}_k)_{\alpha_k} \tag{51}$$

In the IPA, the TPA appear when 2ω coincides with the poles of $\chi_0^{(k)}$, which are the orbital energy differences in the static Kohn-Sham calculation.

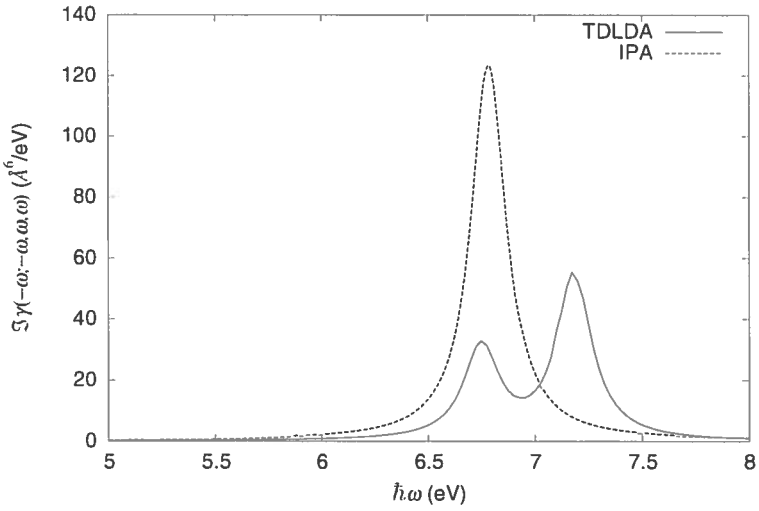

Fig. 4. Imaginary part of the hyperpolarizability $\gamma(-\omega;-\omega,\omega,\omega)$ of Ar atom. The solid line is the present result, and dashed line is a result of calculation with independent particle approximation (IPA) (see text). The prominent peaks correspond to two-photon absorption transitions from the ground $^1S^e$ state to excited even-parity states.

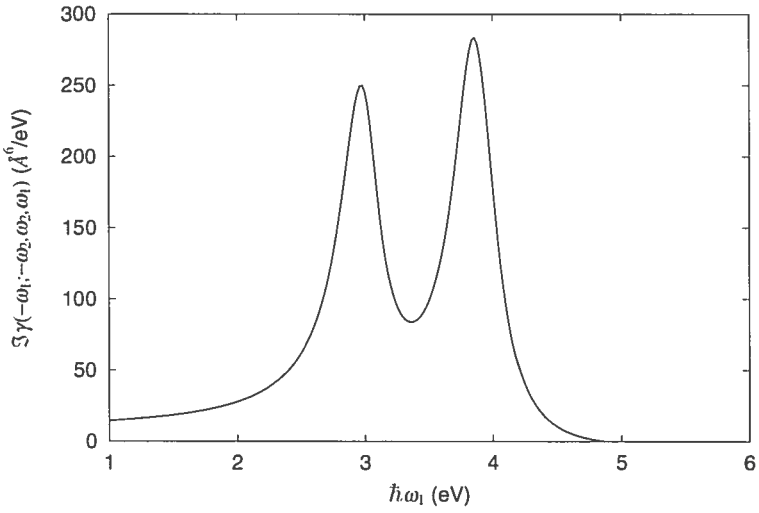

Fig. 5. Imaginary part of the hyperpolarizability $\gamma(-\omega_1;-\omega_2,\omega_2,\omega_1)$ of Ar atom. $\hbar\omega_2$ is fixed at 10.49 eV.

In Fig. 4, one prominent peak is seen in the IPA calculation, and two peaks in the TDDFT. The energy of the IPA peak locates at 6.78 eV which is half of the energy difference between $3p$ and $4p$ orbitals in the static Kohn-Sham calculation. In the TDDFT calculation, two peaks appear at 6.75 and 7.2 eV. We show in Table 1 the excitation energies of $^1S^e$ and $^1D^e$ states of Ar atom in the TDDFT calculation as well as measured values. The peak positions in the response calculation shown in Fig. 4 coincide with half of the excitation energies in the TDDFT with LB94. The dynamical screening effect included in the TDDFT calculation thus splits the strength of the TPA of $3p \rightarrow 4p$ transition into two multiplets of $^1S^e$ and $^1D^e$ states. The integrated strength of the two peaks in TDDFT is somewhat smaller than that of IPA.

Table 1
Excitation energies of Ar atom obtained by the TDDFT calculation and measurements [28]. In the TDDFT, two kinds of exchange-correlation potentials, simple LDA and the LB94 functional [27], are employed. The unit is in eV

state	LB94	LDA	EXP.
$^1D_2^e$	13.50	12.35	13.17
$^1S_0^e$	14.37	13.03	13.48

Table 2
Two-photon transition rate constants in unit of cm^{4}s between the ground state and $^1D_2^e$ and $^1S_0^e$ states of Ar atom

state	present	CCSD[a]	MCSCF[b]	EXP.[c]
$\hbar\omega_1 = \hbar\omega_2$				
$^1D_2^e$	0.55×10^{-51}	0.412×10^{-51}	0.426×10^{-51}	
$^1S_0^e$	0.99×10^{-51}	3.04×10^{-51}		
$\hbar\omega_2 = 10.49$(eV)				
$^1D_2^e$	11×10^{-51}	1.83×10^{-51}	1.91×10^{-51}	2.05×10^{-51}
$^1S_0^e$	14×10^{-51}	9.52×10^{-51}		

[a] from Ref. [29], [b] from Ref. [30].
[c] from Ref. [31].

We also carried out calculations of the TPA for two-color laser field, $\gamma(-\omega_1; -\omega_2, \omega_2, \omega_1)$ with $\hbar\omega_1 \neq \hbar\omega_2$. The measurements and results of other calculations are available for the case of $\hbar\omega_2 = 10.49$ eV. In Fig. 5, we show the TDDFT results where $\hbar\omega_1$ is varied. There appear peaks at $\hbar\omega_1 = 2.98$ eV and 3.86 eV. The summed energies, $\hbar\omega_1 + \hbar\omega_2$, coincide with the excitation energies of $^1S^e$ and $^1D^e$ states. The shape of the spectra is seen to be quite different from the degenerate type TPA spectra of Fig. 4. Especially, the peak intensities are substantially enhanced, about 5 times larger than the degenerate case.

In Table 2, we show the TPA strength obtained by the present calculation and compare it with measurements and other calculations. The TPA strength is defined by

$$K = \frac{2\pi^2\hbar\omega^2}{c^2}\frac{1}{2R_y}\int_\Gamma d(\hbar\omega)\mathrm{Im}[\chi^{(3)}(-\omega; -\omega, \omega, \omega)] \tag{52}$$

and

$$K = \frac{4\pi^2\hbar\omega_1\omega_2}{c^2}\frac{1}{2R_y}\int_\Gamma d(\hbar\omega_1)\mathrm{Im}[\chi^{(3)}(-\omega_1; -\omega_2, \omega_2, \omega_1)] \tag{53}$$

where R_y is the Rydberg constant, and the integration is performed in the region around a resonance peak.

We find common features between the TDDFT and CCSD calculations: The TPA strength of $^1S^e$ state is larger than that of $^1D^e$. The TPA strength with two-color laser ($\hbar\omega_1 \neq \hbar\omega_2$) is much larger than the strength with the monochromatic laser ($\hbar\omega_1 = \hbar\omega_2$) in both calculations. However, the difference of strengthes between the $^1S^e$ and $^1D^e$ transitions is much smaller in the TDDFT calculation than those in the CCSD calculation. The experimental value is reported for $^1D^e$ transition in two-color measurement, which agrees well with CCSD and MCSCF calculations and is five times smaller than the TDDFT result.

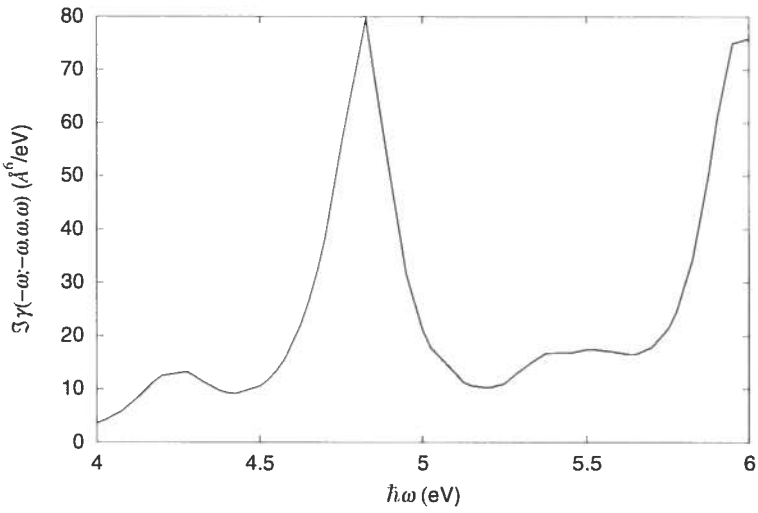

Fig. 6. Imaginary part of the second-hyperpolarizability of ethylene molecule.

5.2. *Ethylene molecule*

We next show the TPA spectra of ethylene molecule in the TDDFT. This molecule has many electronic excited states below the ionization threshold. The $\pi \rightarrow \pi^*$ excited states appear at 4.36 eV (triplet) and 7.6 eV (singlet), and their symmetries are assigned as B_{1u}. Since the ground state of the ethylene molecule has $^1A_{1g}$ symmetry, vertical electronic transitions to the $\pi \rightarrow \pi^*$ excitations and other ungerade states are forbidden in the TPA. The TPA transitions to the gerade states, $\pi \rightarrow p$ and $\pi \rightarrow f$ Rydberg states, are allowed.

The linear optical absorption in the ethylene molecule in the TDDFT was reported in Ref. [14], in which the measured spectra are excellently reproduced by the calculation. In view of this success in the one-photon absorption, we think the two-photon absorption in the ethylene molecule will give a good opportunity to examine accuracy of the TDDFT for the TPA. Unfortunately, we could not find any experimental report.

The TDDFT calculation is achieved employing a grid points inside a sphere of 6 Å radius with 0.3 Å grid spacing. The LB94 exchange-correlation potential is utilized. In Figs 6 and 7, the imaginary and the real parts of the hyperpolarizability, $\gamma(-\omega;-\omega,\omega,\omega)$, are shown. The average over orientation of the molecule is taken into account. Several structures are seen in the TPA, namely, the imaginary part of $\gamma(-\omega;-\omega,\omega,\omega)$, below half of the ionization potential (11.7 eV in the calcualtion and 11.0 eV in the measurements). In the real part, an enhancement is seen at the frequency where substantial TPA is observed. A substantial peak appears at 4.83 eV in the imaginary part. At twice of this energy 9.6 eV, we found $2A_g$ state appear in the TDDFT excitation energy calculation [32,33]. This state is known to appear at 8.29 eV in the measurement. The calculated excitation energy of this state is too high by 1.3 eV. This state is a π to Rydberg p_x transition [34,35]. Weak features are seen around 4.3 and 5.5 eV. At twice of these energies, several excited states can be found in the TDDFT excitation energy calculation, and they are gerade states which are forbidden by one photon absorption transitions.

Summarizing this section, the hyperpolarizability in the complex energy plane can be calculated in the uniform grid representation in the perturbative formalism with the modified Sternheimer method. Since measurements of the TPA is rather limited, it is at this stage difficult to make an assessment on the accuracy of the TDDFT for the TPA.

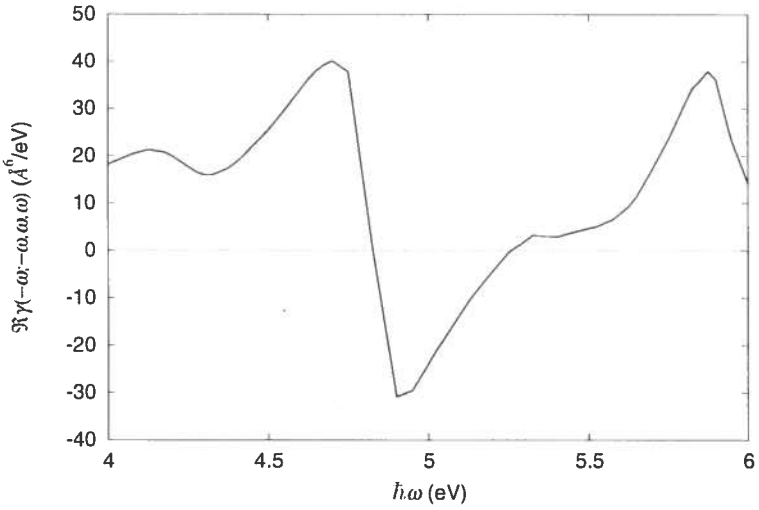

Fig. 7. Real part of the second-hyperpolarizability of ethylene molecule.

6. Summary

We present real-space computational methods for linear and nonlinear polarizabilities based on the time-dependent density-functional theory. The real-space method implies usage of the uniform grid representation in the three-dimensional Cartesian coordinates. The wave functions are expressed with their values on the grid points. Two distinct methods are discussed, the real-time method and the perturbative formalism with the modified Sternheimer method.

The real-time, real-space method has been most successful for calculations of linear polarizability. In this article, we have shown that the real-time method is also useful for the calculations of nonlinear polarizabilities. Since the method does not require any perturbative expansion, this approach is much simpler in both formalism and programming than the perturbative method.

The uniform grid representation also provides efficient representation to solve the response equations, in which the integral equations are converted into equivalent differential equations. We have shown that the nonlinear polarizabilites in the complex frequency plane can be efficiently calculated. To demonstrate it, the two-photon absorption cross sections which is related to the imaginary part of the hyperpolarizability are analyzed.

Acknowledgments

K.Y. acknowledges support by the Ministry of Education, Culture, Sports, Science and Technology of Japan, Contract No. 14540369. G.B. also acknowledges support by the US Department of Energy under Grant DE-FG03-00-ER41132 and the Computational Materials Science Network. The authors acknowledge the Institute for Solid State Physics, Univ. of Tokyo, the Institute of Physical and Chemical Research (RIKEN), for the use of supercomputers.

References

[1] A. Zangwill and P. Soven, *Phys. Rev.* **A21** (1980), 1561.

[2] G. Senatore and K.R. Subbaswamy, *Phys. Rev.* **A35** (1987), 2440.
[3] K. Yabana and G.F. Bertsch, *Phys. Rev.* **B54** (1996), 4484.
[4] J.-I. Iwata, K. Yabana and G.F. Bertsch, *J. Chem. Phys.* **115** (2001), 8773.
[5] S.J.A. van Gisbergen, J.G. Snijders and E.J. Baerends, Phys. Rev. Lett. **78**, 3097 (1997).
[6] S.J.A. van Gisbergen, J.G. Snijders and E.J. Baerends, *J. Chem. Phys.* **109** (1998), 10644; (erratum) **111** (1999), 6652.
[7] H.H. Henze, F. Della and A. Görling, *J. Chem. Phys.* **116** (2002), 9624.
[8] P. Salek, O. Vahtras, T. Helgaker and H. Ågren, *J. Chem. Phys.* **117** (2002), 9630.
[9] E.K.U. Gross, J.F. Dobson and M. Petersilka, *Density Functional Theory*, Springer Series Topics in Current Chemistry, edited by R.F. Nalewajski (Springer, Heidelberg, 1996), p. 81.
[10] K. Yabana and G.F. Bertsch, *Int. J. Quantum Chem.* **75** (1999), 55.
[11] G.F. Bertsch and K. Yabana, Density functional theory, in: *Introduction to Modern~@Methods of quantum many-body theory and their applications*, A. Fabrocini, S. Fantoni and E. Krotscheck, eds, (World Scientific, 2002), pp. 1–48.
[12] K. Yabana and G.F. Bertsch, *Phys. Rev.* **A60** (1999), 1271.
[13] G.F. Bertsch, J.-I. Iwata, A. Rubio and K. Yabana, *Phys. Rev.* **B62** (2000), 7998.
[14] T. Nakatsukasa and K. Yabana, *J. Chem. Phys.* **114** (2001), 2550.
[15] P.N. Butcher and D. Cotter, *The Elements of Nonlinear Optics*, Cambridge University Press, Cambridge, 1990.
[16] W. Ekardt, *Phys. Rev.* **B29** (1984), 1558.
[17] G.F. Bertsch, *Comp. Phys. Comm.* **60** (1990), 247.
[18] G.D. Mahan, *Phys. Rev.* **A22** (1980), 1780.
[19] N. Troullier and J. Martins, *Phys. Rev.* **B44** (1991), 1993.
[20] L. Kleinman and D. Bylander, *Phys. Rev. Lett.* **48** (1982), 1425.
[21] J.R. Chelikowsky, N. Troullier, K. We and Y. Saad, *Phys. Rev.* **B50** (1994), 11355.
[22] H. Flocard, S.E. Koonin and M.S. Weiss, *Phys. Rev.* **C17** (1978), 1682.
[23] R. Brett et al., *Templates for the Solution of Linear Systems: Building Blocks for Iterative Methods*, Society for Industrial and Applied Mathmatics, Philadelphia, 1994.
[24] J. Guan, P. Duffy, J.T. Carter, D.P. Chong, K.C. Casida, M.E. Casida, M. Wrinn, *J. Chem. Phys.* **98** (1993), 4753.
[25] J.P. Perdew and A. Zunger, *Phys. Rev.* **B23** (1981), 5048.
[26] F. Calvayrac, P.G. Reinhard, E. Suradud, C.A. Ullrich, Phys. Rep. **337**, 493 (2000).
[27] R. van Leeuwen and E.J. Baerends, *Phys. Rev.* **A49** (1994), 2421.
[28] C.E. Moore, *Natl, Bur. Stand. (U.S.) Circ.* **467** (1949), 212.
[29] C. Hätting, O. Christiansen and P. Jorgensen, *J. Chem. Phys.* **108** (1998), 8355.
[30] D. Sundholm, A. Rizzo and P. Jorgensen, *J. Chem. Phys.* **101** (1994), 4931.
[31] M.P. McCann, C.H. Chen and M.G. Payne, *J. Chem. Phys.* **89** (1988), 5429.
[32] M.E. Casida, in: *Recent Advances in Density Functional Methods, Part I*, D.P. Chong, ed., Singapore, World Scientific, 1995, p. 155.
[33] A. Muta, J.-I. Iwata, Y. Hashimoto and K. Yabana, *Prog. Theor. Phys.* **108** (2002), 1065.
[34] K.B. Wiberg et al., *J. Phys. Chem.* **96** (1992), 10756.
[35] P.R. Schipper et al., *J. Chem. Phys.* **112** (2000), 1344.